



PERGAMON

Solid State Communications 114 (2000) 271–276

solid
state
communications

www.elsevier.com/locate/ssc

X-ray standing-wave analysis of the rare-earth atomic positions in $\text{RBa}_2\text{Cu}_3\text{O}_{7-\delta}$ thin films

A. Kazimirov^a, L.X. Cao^b, G. Scherb^b, L. Cheng^a, M.J. Bedzyk^{a,c}, J. Zegenhagen^{b,d,*}^aMaterial Science Department, Northwestern University, Evanston, IL, USA^bMax-Planck-Institut für Festkörperforschung, Stuttgart, Germany^cMaterial Science Division, Argonne National Lab., Argonne, IL, USA^dEuropean Synchrotron Radiation Facility, B.P. 220, F-38043 Grenoble Cedex, France

Received 13 January 2000; accepted 24 January 2000 by M. Cardona

Abstract

We applied the X-ray standing-wave technique to study the lattice location of rare-earth atoms in thin films of $\text{RBa}_2\text{Cu}_3\text{O}_{7-\delta}$ ($R = \text{Gd}, \text{Pr}$). The films had a thickness of 200 nm and were grown by pulsed laser deposition on $\text{SrTiO}_3(001)$ substrates. The standing wave was generated by kinematic Bragg diffraction. The angular dependence of the R–L and Ba–L fluorescence yield was recorded while scanning through the (005) Bragg reflection of the film. Analysis of the angular dependence leads to information on the degree of site interchange of R and Ba. We found a clear indication that Pr substitutes for Ba. © 2000 Elsevier Science Ltd. All rights reserved.

Keywords: High- T_c superconductors; B. Epitaxy; C. X-ray scattering

1. Introduction

Despite the passage of almost 15 years since the initial discovery by Bednorz and Müller [1], high-temperature superconductors (HTS) are still the subject of intense research activities. This is jointly motivated by the expected technical applications and by the fact that the basic mechanism of superconductivity is not yet resolved. One important means of either obtaining clues toward the mechanism of superconductivity or to optimize the material parameters (e.g. the transition temperature) has always been via a systematic elemental (or isotopic) substitution method. For the 90 K HTS $\text{YBa}_2\text{Cu}_3\text{O}_{7-\delta}$ it was found that Y can be substituted by nearly all rare-earth atoms with little effect on the properties of the material. Only for the exchange of Y by Ce and Tb does the material not form the orthorhombic 123 structure of the 90 K $\text{RBa}_2\text{Cu}_3\text{O}_{7-\delta}$ ($R = \text{Y}$ or rare-earth atoms) compound shown in Fig. 1. In all other cases, the elemental replacement results in the 123 structure and has

insignificant influence on the superconducting properties of the 123 compound with the possible exception of Pr. Despite the fact that $\text{PrBa}_2\text{Cu}_3\text{O}_{7-\delta}$ exhibits the 123 structure it has generally, at least until recently, been reported as being non-superconducting. (There are recently several reports about superconducting PrBCO, e.g. [2,3]. However, the structure and stoichiometry of the superconducting phase thus far remains unclear.) Several models have been put forward to explain this puzzle. Most of them assume, as a starting point, an average valence for the Pr of $+(3+x)$ (in contrast to Y^{3+}) and thus an influence on the hole concentration in the CuO_2 planes. A widely known model for the explanation of the non-superconducting properties of PrBCO is that of Fehrenbacher and Rice [4], based on an exclusively electronic origin; a mixed valent Pr ion leads to a rehybridization of the oxygen atoms in the CuO_2 planes. There are, however, other proposals, invoking structural changes as the underlying cause. One of them assumes disorder on the Pr site [5], whereas the other postulates that a significant fraction of Pr ions are sitting on Ba sites [6]. Whether any of these models are the key to or at least of relevance for the non-superconducting behavior of PrBCO is not clear. However, the open questions of the crystal (or defect) structure of the PrBCO compound should be answered by proper

* Corresponding author. European Synchrotron Radiation Facility, BP 220, F-38043 Grenoble Cedex, France. Fax: +33-476-882-160.

E-mail address: zegenhagen@esrf.fr (J. Zegenhagen).

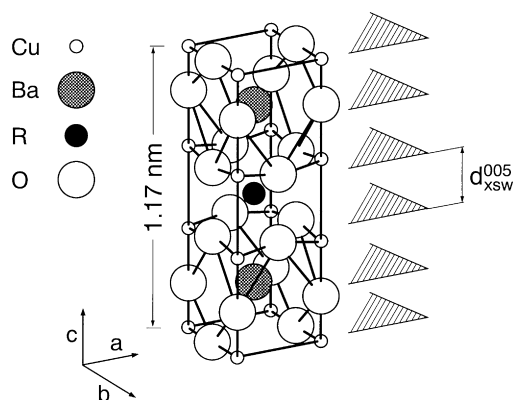


Fig. 1. The orthorhombic unit cell of the $\text{RBa}_2\text{Cu}_3\text{O}_{7-\delta}$ high- T_c superconductor. The (005) diffraction planes are indicated on the right-hand side.

experimental investigations. This task is difficult; while there are recent reports supporting the assumption of rare-earth atoms substituting on Ba sites [7,8], others are ruling this out [9,10]. A decisive answer can possibly not be given in a unique way since the occurrence of a place exchange of rare-earth ions and Ba or the substitution of rare-earth ions on Ba sites may depend on specific details of the sample preparation. To date, primarily, bulk crystals have been investigated. In the present study we apply the X-ray standing-wave (XSW) method to the analysis of the occupation of rare-earth atoms on Ba sites in ultra thin films grown by laser deposition.

The XSW method is based on the generation of a standing-wave field by the superposition of two plane and coherent X-ray waves created by Bragg diffraction. Traversing the range of total reflection by tuning either the angle of incidence or the X-ray energy, the XSW can be shifted in a controlled way. The strength of the photoelectric scattering of atoms within the range of the wavefield is proportional to the wavefield intensity at the position of those atoms. Thus, monitoring photoelectrons or X-ray fluorescence (or other decay channels) while shifting the wavefield, atomic positions can be deduced by analyzing the scattering response as a function of angle or energy. Since we employ spectroscopic techniques, the analysis of the signal is element specific. XSW has been successfully employed not only for surface structural analysis [11] but also for bulk crystals as proven in its first demonstration [12].

Typically, Bragg diffraction from perfect single crystals is employed to generate the interference field and the dynamical theory of X-ray diffraction [13,14,15] is used for the analysis of the data. Since the range of Bragg total reflection covers only some (10) μrad , the perfection of the sample crystals has been, for a long time, the main obstacle to the application of the method for the study of structural details of HTS materials. Recently, a novel modification of the XSW method, based on the excitation of an XSW inside a

thin epitaxial film, has been used [16,17]. In this case, a weak beam, kinematically diffracted from the film, interferes with the strong incident beam resulting in a very weak spatial contrast of the interference field with a modulation of the interference fringes in the % range, depending on the thickness and perfection of the film. This disadvantage in intensity contrast is offset by the fact that the intrinsic angular width of the reflection curve is inversely proportional to the film thickness and can thus easily exceed several mrad. We demonstrated this method for the analysis of the Sm lattice site in a 150 nm thick $\text{SmBa}_2\text{Cu}_3\text{O}_{7-\delta}$ film on $\text{SrTiO}_3(001)$ [16] and later for the determination of the polarity of a GaN thin film grown on $\text{Al}_2\text{O}_3(0001)$ [17]. Here we employ this method to study the occupancy of lattice sites by rare-earth and Ba atoms in 123 compounds.

2. Experiment

The $\text{GdBa}_2\text{Cu}_3\text{O}_{7-\delta}$ (GdBCO) and $\text{PrBa}_2\text{Cu}_3\text{O}_{7-\delta}$ (PrBCO) films with thickness of 200 nm were grown on $\text{SrTiO}_3(001)$ substrates using pulsed laser deposition [18,19]. The GdBCO was superconducting, exhibiting a sharp transition with $T_{c,0}$ above 90 K, whereas the PrBCO showed semiconducting behavior.

The XSW measurements were performed at the X15A beam line [11] of the NSLS and BNL. The energy of the incident X-ray beam was tuned to 8.0 keV, i.e. below the Cu-K (8.979 keV), edge using a Si(111) double crystal monochromator. The (005) reflection from the film was chosen for the XSW measurements for three reasons: it is one of the strongest reflections for the 123 structure; in the wider range of the momentum transfer vector, chosen for the RBCO(005) reflection, there are no substrate reflections that could possibly interfere with the incident X-ray beam; for the (005) reflection the scattering amplitudes from the Ba and rare-earth atomic planes are out of phase (nearly by π) and thus, as a function of incident angle θ , the fluorescence yield functions from the rare-earth atoms and Ba atoms are phase shifted by the same amount, resulting in a high sensitivity for the detection of interchange of their sites.

The samples were mounted on a two-circle diffractometer and fluorescence spectra were recorded as a function of θ with an energy-dispersive solid state detector (SSD). Simultaneously, the intensity of the reflected X-ray beam was monitored [11].

The fluorescence spectra were then analyzed to extract the fluorescence signals specific to the rare-earth and Ba atoms. For the GdBCO film the $\text{Ba-L}_{\alpha 1}$ and the $\text{Gd-L}_{\alpha 1}$ lines and for the PrBCO film the $\text{Ba-L}_{\alpha 1}$ and the $\text{Pr-L}_{\beta 1}$ lines were chosen. Owing to the moderate energy resolution (≈ 180 eV) of the SSD, fluorescence lines from different elements could not always be separated. Care was taken to minimize this effect or to take it correctly into account.

In order to minimize the contribution of the Ti-K $_{\alpha}$ fluorescence from the substrate, and to reduce the potential

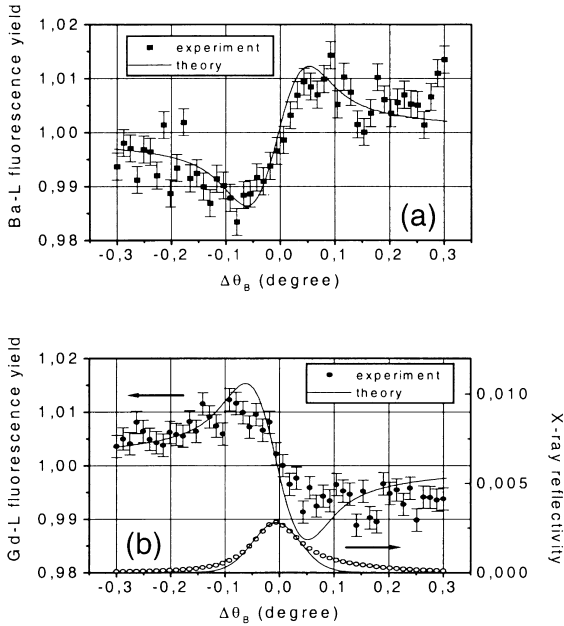


Fig. 2. (a) The experimental Ba–L_{α1}. (b) The Gd–L_{α1} fluorescence yields and the rocking curve measured from the 200 nm thick GdBa₂Cu₃O_{7–δ} film. The solid lines represent the theoretical yield functions calculated for the ideal 123 structure.

overlap with the Ba–L_α signal, the fluorescence spectra were recorded at glancing take-off angle $\alpha \leq 1.4^\circ$. By measuring spectra from the bare substrate and from samples with films of the same composition but different thickness, the contribution of the Ti–K_α fluorescence was estimated to be 13%. This contribution is constant with θ and thus the Ba yield curve can be easily corrected. The experimental Gd–L_{α1} yield measured from the GdBCO 200 nm thick film is shown in Fig. 2 together with the corrected Ba–L_{α1} data.

The angular, i.e. θ -dependent Ba–L_{α1} and Pr–L_{β1} yield for the 200 nm thick PrBCO film are shown in Fig. 3. The Ba–L_{α1} yield was corrected in the described way for the GdBCO sample. The Pr–L_{β1} line could not be separated from the (much weaker) Ba–L_{γ1} line. However, by determining the relative intensities of all of the Ba–L lines using the spectra from the GdBCO samples, where all the lines can be distinguished, the Ba–L_{γ1} contribution was estimated to contribute 14% to the Pr–L_{β1} line. Since both the Ba and Pr signals are a function of θ , the experimental Pr fluorescence data were fitted by the function $Y_{Pr} = 0.86Y_{theo,Pr} + 0.14Y_{theo,Ba}$, where $Y_{theo,(Pr,Ba)}$ describes calculated yield curves (see below) for the ideal location of Pr and Ba.

3. Discussion

The fluorescence yield from the (near) surface layer of a compound crystal excited by the XSW from the sublattice of

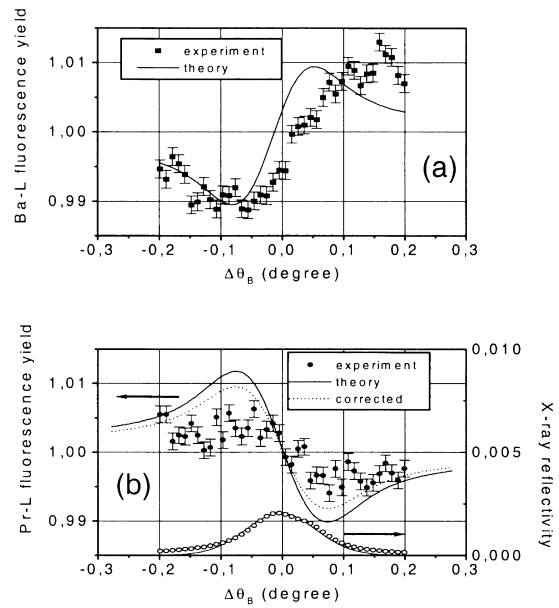


Fig. 3. (a) The experimental Ba–L_{α1}. (b) The Pr–L_{β1} fluorescence yields and the rocking curve measured from the 200 nm thick PrBa₂Cu₃O_{7–δ} film. The solid lines represent the theoretical yield functions calculated for the ideal 123 structure. The dashed curve shows the curve described by $Y = 0.86Y_{theo,Pr} + 0.14Y_{theo,Ba}$ which takes into account the contribution of the weak Ba–L_{γ1} lines to the Pr signal.

a certain element j employing a diffraction vector \mathbf{H} can be written as [20–22]

$$Y_j^H(\theta) = 1 + R(\theta) + 2\sqrt{R(\theta)} \sum_{i=1}^N \cos(\nu(\theta) - \mathbf{H} \cdot \mathbf{r}_{j,i}) \quad (1)$$

where the sum is carried out over all N atoms of the element j within the interference field. Here, $\nu(\theta)$ is the phase of the complex ratio E_r/E_o , i.e. the ratio of the electric field amplitudes of the reflected and the incident X-ray waves, $R = |E_r/E_o|^2$ is the reflectivity and $\mathbf{r}_{j,i}$ are the positions of the atoms of element j . For the case in which these atoms occupy n_A positions in the unit cell Eq. (1) becomes

$$Y_j^H(\theta) = 1 + R(\theta) + 2\sqrt{R(\theta)} e^{-M_j^H - W_j^H} \sum_i^{n_A} \cos(\nu(\theta) - P_{j,i}^H), \quad (2)$$

where M_j^H and W_j^H represent the thermal and static Debye–Waller factors, $P_{j,i}^H = \mathbf{H} \cdot \mathbf{r}_{j,i}$ and $n_A = 1, 2$ for R and Ba, respectively, for the ideal orthorhombic unit cell of RBCO. This can finally be written as

$$Y_j^H(\theta) = 1 + R(\theta) + 2\sqrt{R(\theta)} |A_j^H| e^{-M_j^H - W_j^H} \cos(\nu(\theta) - P_{j,i}^H) \quad (3)$$

where $|A_j^H|$ and $P_{j,i}^H$ are the amplitude and the phase of the Fourier coefficient of the atoms of the (ideal) sublattice of

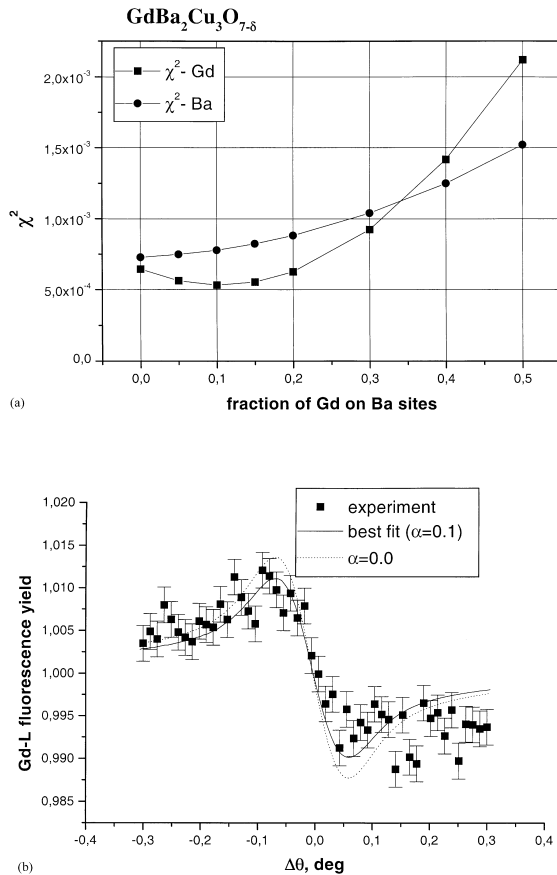


Fig. 4. (a) χ^2 values for fits to the Gd-fluorescence and the Ba-fluorescence for fractional place exchange between Gd and Ba in the GdBCO thin film. (b) Gd-fluorescence yield. Points represent the experimental data, the solid line the best fit for a fractional substitution of Ba sites by Gd with $\alpha = 0.1$, and the dashed line the fit with $\alpha = 0$.

element j [20,21]. The amplitude and phase of the Fourier coefficient of the j th sublattice enter directly into the third interference term of Eq. (3), thus rendering the XSW method phase sensitive, in contrast to standard diffraction techniques. Theoretical yield curves for Pr, Gd and Ba, calculated using an algorithm based on the dynamical diffraction theory for multilayer crystalline system [22], are shown in Figs. 2 and 3. These calculations were performed for the ideal 123 structure without any fitting parameters, using only a Gaussian convolution to account for some mosaic spread in the films. The calculated curve for the Ba yield from the GdBCO film (Fig. 2) agrees very well with the experimental curve while for the Gd the experimental curve exhibits a smaller modulation. For the Pr yield the experimentally observed XSW modulation is half as strong as calculated.

We assume next that a fraction of the rare-earth atoms occupy Ba sites and a fraction of the Ba atoms occupy rare-

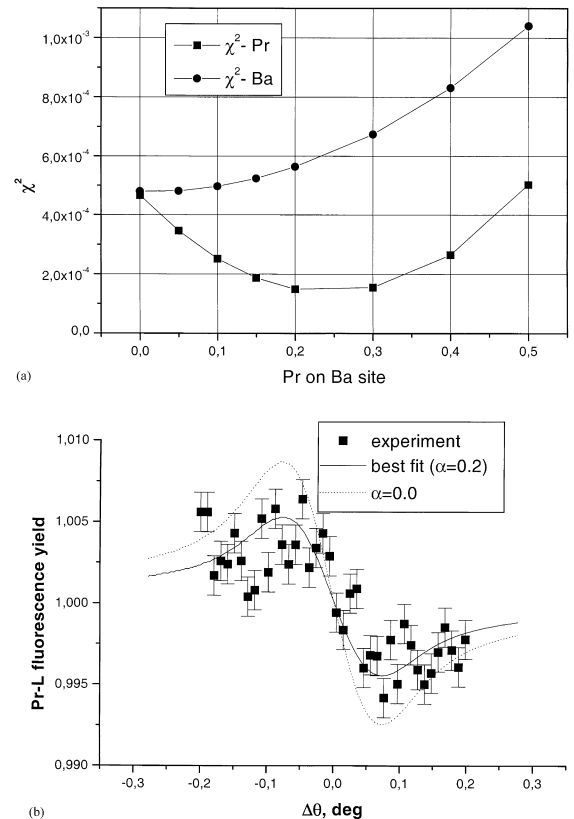


Fig. 5. (a) χ^2 values for fits to the Pr-fluorescence and the Ba-fluorescence for fractional place exchange between Pr and Ba in the PrBCO thin film. (b) Pr-fluorescence yield. Points represent the experimental data, the solid line the best fit for a fractional occupancy of Ba sites by Pr with $\alpha = 0.2$, and the dashed line the fit with $\alpha = 0$.

earth sites in an otherwise unchanged RBCO structure. The corresponding yield curves for Pr and Gd were calculated with a fraction α of the rare-earth atoms on Ba-sites and the remainder $1 - \alpha$ on the regular rare-earth sites. Similarly, yield curves were calculated for the Ba fluorescence yield with a fraction of the Ba atoms occupying rare-earth sites and the remaining Ba atoms on their usual lattice sites. Figs. 4(a) and 5(a) show the improvement in χ^2 for the corresponding fits to the experimental yield curves as a function of this fractional occupation for the GdBCO and the PrBCO film, respectively. The best fits are drawn as solid lines in the Figs. 4(b) and 5(b) for the GdBCO and the PrBCO film, respectively. For Fig. 4(a), the χ^2 -minimum occurs for the Gd-fluorescence yield at a 10% fractional occupation of the Ba sites by Gd. For Pr (Fig. 4(a)), the minimum occurs at the significantly larger value of 20%. However, both minima are not very deep and we can estimate error bars in the fractional occupancy to be 0.1. The minimum of χ^2 for the fractional occupancy of Pr site by Ba is in both cases close to 0% (cf. Figs. 4(a) and 5(a)).

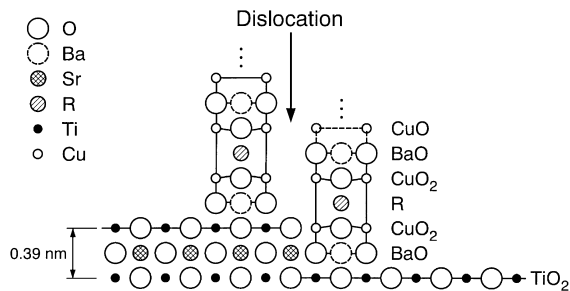


Fig. 6. A sketch of how a slip dislocation is created in the epitaxial thin film on SrTiO₃(001) at a substrate step edge.

The above values are rather large compared to published values for the possible substitution of different rare-earth atoms on Ba sites in the % range (see e.g. Refs. [6,7] and references therein) in bulk single crystals. However, the margin of error is also large and, furthermore, the microscopic or defect structure of thin films is, in several aspects, different from the structure of bulk crystals (or powder samples). Not only the crystal structure of the underlying substrate but also its surface morphology, notably steps, may influence the film structure. Since steps on the SrTiO₃(001) surface exhibit a height of 0.39 nm, about one-third of the *c*-axis lattice constant of the 123 compounds (1.17 nm), (most) steps will lead to dislocations (similar to slip dislocations) in the thin film. (Annealed SrTiO₃(001) surfaces are TiO_x terminated and exhibit predominantly one unit cell, i.e. 0.39 nm-high steps [23].) The thin film can overgrow step edges by adopting a different stacking sequence on top of and below the step edge [23,24], and with increasing film thickness the number of the planar defects originating from substrate steps will be further reduced by a variable, non-unit cell growth mode [25]. In Fig. 6 the generation of such a defect is depicted. The defect results in an effective place exchange of the rare-earth atom and Ba within some restricted area. The presence of these defects has been confirmed by high-resolution transmission electron microscopy [26]. From the discussion above, it is clear that the density of these defects depends on the step density of the substrate and on the film thickness. It is important to mention that the substrates used for the growth of the GdBCO and the PrBCO films were equivalent and the film thickness was the same. Thus, although this type of slip dislocation inhibits a direct interpretation of the individual XSW result in terms of the amount of substitution of the Ba by rare-earth atoms, the comparison of the data for the GdBCO and PrBCO films is meaningful and we may conclude that the Pr exhibits a significantly higher tendency to occupy Ba sites than the Gd. Our results provide evidence that the rare-earth atoms may occupy Ba sites but that Ba atoms do not necessarily move to the rare-earth sites. This indicates that the model of site switching of the two atomic species without any other influence on the structure of the RBCO thin film is oversimplified. For a more detailed

analysis of the microscopic film structure further investigations are necessary.

4. Conclusions

We have found strong evidence of Pr substituting for Ba sites in laser-deposited thin films of the RBCO HTS. For a detailed analysis of the thin film structure further studies are necessary, in particular using well-oriented substrate crystals with an extremely low miscut to avoid slip dislocations originating from steps on the substrate surface.

Acknowledgements

Valuable discussions with M. Cardona, C. Bernhard, A. Shukla, K. Oka and S. Jandl are gratefully acknowledged. Expert technical assistance by W. Stiepany was instrumental for this study. We are grateful to V.G. Kohn for providing the computer code for the XSW analysis in layered crystals and to the staff of the NSLS for assistance on the floor. This project was supported by the German BMBF under contract 13N5840 and 05-622GUA-1, by the US Department of Energy under contracts W-31-109-ENG-38 to ANL, and DE-AC02-98CH10886 to BNL, and by NSF under contract DMR09973436 to M.J.B.

References

- [1] J.G. Bednorz, K.A. Müller, *Z. Phys. B* 64 (1986) 189.
- [2] H.A. Blackstead, J.D. Dow, D.B. Chrisey, J.S. Horowitz, M.A. Black, P.J. McGinn, A.E. Klunzinger, D.B. Pulling, *Phys. Rev. B* 54 (1996) 6122.
- [3] Z. Zou, J. Ye, K. Oka, Y. Nishihara, *Phys. Rev. Lett.* 80 (1998) 1074.
- [4] R. Fehrenbacher, T.M. Rice, *Phys. Rev. Lett.* 70 (1993) 3471.
- [5] A.I. Liechtenstein, I.I. Mazin, *Phys. Rev. Lett.* 74 (1995) 1000.
- [6] H.A. Blackstead, J.D. Dow, *Phys. Lett. A* 206 (1995) 107.
- [7] A. Shukla, B. Barbiellini, A. Erb, A. Manuel, T. Buslaps, V. Honkimäki, P. Suortti, *Phys. Rev. B* 59 (1999) 12 127.
- [8] A.A. Martin, T. Ruf, M. Cardona, S. Jandl, D. Barba, V. Nekvasil, M. Divis, T. Wolf, *Phys. Rev. B* 59 (1999) 6528.
- [9] C.K. Lowe-Ma, T.A. Vanderah, *Physica C* 201 (1992) 233.
- [10] V.G. Harris, D.J. Fatemi, V.M. Browning, M.S. Osofsky, T.A. Vanderah, *J. Appl. Phys.* 83 (1998) 6783.
- [11] J. Zegenhagen, *Surf. Sci. Rep.* 18 (1993) 199.
- [12] B.W. Batterman, *Phys. Rev. Lett.* 22 (1969) 703.
- [13] M. von Laue, *Exakt. Naturwiss.* 10 (1931) 133.
- [14] M. von Laue, *Röntgenstrahlinterferenzen*, 3rd ed., Akademie Verlagsgesellschaft, Frankfurt, 1960.
- [15] B.W. Batterman, H. Cole, *Rev. Mod. Phys.* 36 (1964) 681.
- [16] A. Kazimirov, T. Haage, L. Ortega, A. Stierle, F. Comin, J. Zegenhagen, *Solid State Commun.* 104 (1997) 347.
- [17] A. Kazimirov, G. Scherb, J. Zegenhagen, T.-L. Lee,

- M.J. Bedzyk, M.K. Kelly, H. Angerer, O. Ambacher, J. Appl. Phys. 84 (1998) 1703.
- [18] Q.D. Jiang, K.G. Huang, M. Rao, J. Zegenhagen, J. Phys. C 235–240 (1994) 677.
- [19] Q.D. Jiang, J. Zegenhagen, Surf. Sci. 338 (1995) L882.
- [20] N. Hertel, G. Materlik, J. Zegenhagen, Z. Phys. B 58 (1985) 199.
- [21] A. Yu Kazimirov, M.V. Kovalchuk, V.G. Kohn, Sov. Tech. Phys. Lett. 14 (1988) 587.
- [22] V.G. Kohn, M.V. Kovalchuk, Phys. Stat. Sol. A 64 (1981) 359.
- [23] J. Zegenhagen, T. Haage, Q.D. Jiang, Appl. Phys. A 67 (1998) 711.
- [24] J. Zegenhagen, T. Siegrist, E. Fontes, L.E. Berman, J.R. Patel, Solid State Commun. 93 (1995) 763.
- [25] T. Haage, Q.D. Jiang, M. Cardona, H.-U. Habermeier, J. Zegenhagen, Appl. Phys. Lett. 68 (1996) 2427.
- [26] T. Haage, J. Zegenhagen, J.Q. Li, H.-U. Habermeier, M. Cardona, Ch. Jooss, R. Warthmann, A. Forkl, H. Kronmüller, Phys. Rev. B 56 (1997) 8404.